Letter

Electron-phonon interactions in the Andreev bound states of aluminum nanobridge Josephson junctions

James T. Farmer,* Azarin Zarassi, Sadman Shanto, Darian Hartsell,† and Eli M. Levenson-Falk‡
Department of Physics, and Center for Quantum Information Science and Technology, University of Southern California, Los Angeles, California 90089-0484, USA

(Received 30 November 2022; revised 21 March 2023; accepted 5 April 2023; published 27 April 2023)

We report continuous measurements of quasiparticles trapping and clearing from Andreev bound states in aluminum nanobridge Josephson junctions integrated into a superconducting-qubit-like device. We find that trapping is well modeled by independent spontaneous emission events. Above 80 mK the clearing process is well described by the absorption of thermal phonons, but other temperature-independent mechanisms dominate at low temperature. We find a complex structure in the dependence of the low-temperature clearing rate on the Andreev bound state energy. Our results shed light on quasiparticle behavior in qubitlike circuits.

DOI: 10.1103/PhysRevB.107.L140506

Nonequilibrium quasiparticles (QPs) in superconducting quantum circuits can hinder device operation, limiting coherence in most qubit architectures [1,2] and inducing correlated, difficult-to-correct errors across multiple qubits on the same chip [3,4]. The QPs are generated by nonthermal mechanisms such as pair-breaking infrared photons [5] or energy dissipation from local radioactivity and cosmic rays [2]. Significant nonequilibrium QP populations with fractional densities $x_{\mathrm{qp}} \sim 10^{-9}$–$10^{-5}$ are ubiquitously observed [5–8] and have proven difficult to eliminate. Mitigation strategies such as improved light-tight shielding [5], input/output filtering with infrared absorbers [7,9,10], and device engineering [11–17] have reduced QP densities over the last decade. Many works have probed QP populations by detecting single charge tunneling across Josephson junctions [1,7,15,18–22] or observing QPs trapped inside the Andreev bound states (ABS) of a junction [23–27]. These ABS provide a complementary measurement of QP behavior, and can be used as qubit modes themselves [28,29]. In many implementations the ABS qubit relies on a nonequilibrium QP trapping in order to initialize the state; such qubits are vulnerable to additional trapping events and to accidental clearing of the QP from the ABS. There is thus a great need to better understand the behavior of QPs in ABS and the mechanisms for QPs transitions between ABS and bulk continuum states.

In this Letter we investigate the electron-phonon interactions involved in trapping a quasiparticle into and clearing a quasiparticle from an Andreev bound state. We show continuous, real-time measurements of ABS trapping dynamics as a function of ABS energy and device temperature in a superconducting-qubit-like device. We find that QP trapping is consistent with independent spontaneous emission events from a bulk QP population that is a combination of a temperature-independent nonequilibrium background and a thermal equilibrium density. We further find that QP clearing from an ABS is consistent with a process dominated by the absorption of a thermal phonon at temperatures above 80 mK. At low temperatures, we find evidence that the absorption of microwave photons by trapped QPs is the dominant clearing mechanism, even at low drive powers. We analyze the mean QP occupancy of our ABS device and find independent confirmation of our trapping and clearing models. Our results shed light on quasiparticle behavior in ABS and in qubitlike circuits in general.

To study QP trapping, we require a circuit element which is sensitive to the occupation of single electron states with tunability below the superconducting gap. We find such an element in the aluminum nanobridge Josephson junction, an all-superconducting junction which was shown [30–32] to follow the current-phase relation for point contacts derived by Kulik and Omel'Yanchuk [33] while providing several hundred conduction channels. Each conduction channel hosts a pair of ABS with energies

$$E_A(\delta) = \pm\Delta\sqrt{1 - \tau \sin\frac{\delta}{2}} \tag{1}$$

measured from the Fermi energy. The transparency τ is the probability that an incident Cooper pair is transmitted across the junction and δ is the phase bias across the junction; Δ is the superconducting gap. For short ($\lesssim$100 nm) aluminum nanobridges, τ approximately follows a Dorokhov distribution with a strong preference to be 0 or 1 [31,34]. When occupied, each ABS in a given channel carries equal and opposite contributions to the supercurrent. The negative state is usually occupied while the positive state is unoccupied. However, the positive ABS dips below the gap Δ when both δ and τ are nonzero, making it energetically favorable for a quasiparticle above the gap (i.e., in the bulk continuum) to relax into the ABS and become trapped. When this occurs the supercurrent contribution of the given channel is canceled and the channel is "poisoned." This is the mechanism of our

*jtfarmer@usc.edu
†Present address: Georgia Tech Research Institute, Atlanta, Georgia 30332, USA.
‡elevenso@usc.edu

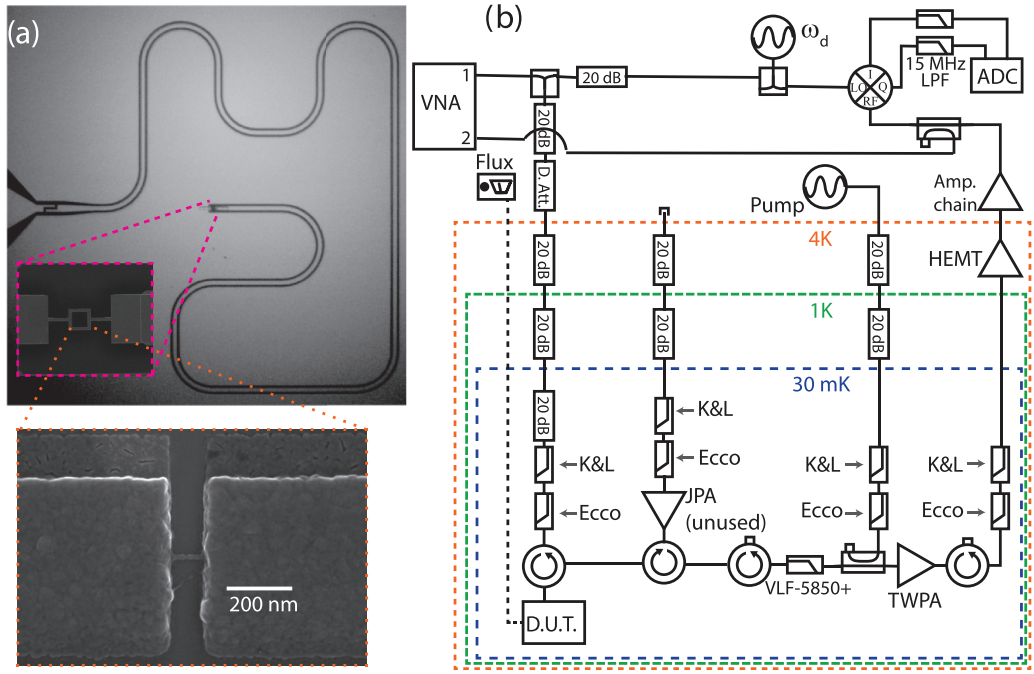

FIG. 1. (a) Images of similar device: A $\lambda/4$ resonator is grounded through a dc SQUID with a pair of symmetric aluminum nanowire junctions. These junctions are approximately 25 nm × 8 nm × 100 nm. (b) The readout drive ω_d is generated at room temperature and attenuated along the path through the dilution refrigerator to the base stage. At 30 mK, pair breaking photons on all inputs and outputs are reduced by K&L 12-GHz low-pass filters and Eccosorb CR110 infrared absorbers. The signal circulates to reflect off our device and pass through a 5.85-GHz low-pass filter. The signal is then amplified by a traveling wave parametric amplifier (TWPA) whose pump is inserted via a directional coupler. The signal exits the dilution refrigerator receiving further amplification by a high-electron-mobility transistor (HEMT) at 4 K and a series of low-noise amplifiers at room temperature. The signal is homodyne demodulated by an IQ mixer and the resulting quadratures are digitized after 15-MHz low-pass filtering. A Keithley source meter sends dc current along the dashed path to a coil in the device package and a vector network analyzer (VNA) is used to measure the resonance as a function of flux.

detection: The Josephson inductance becomes a function of the number of trapped quasiparticles.

By embedding a dc superconducting quantum interference device (SQUID) with symmetric aluminum nanobridge junctions in a $\lambda/4$ coplanar waveguide resonator, we are able to measure the trapping of a QP as a resonant frequency shift of the resonator. This allows for a high-bandwidth, continuous measurement of the ABS occupation in a qubitlike circuit using a standard dispersive measurement setup [27]. A constant flux bias on the SQUID introduces a constant, symmetric phase bias to the junctions $\delta = \pi\phi$ (where ϕ is the applied flux in units of flux quanta), tuning the ABS energies. The fundamental mode $f_0(\phi)$ of our resonator is flux tunable from 4.301 to ∼4.25 GHz with a linewidth $\kappa = 2\pi \times 250$ kHz and the shift due to trapping a single quasiparticle $\chi(\phi)/2\pi$ ranges from 100 to 400 kHz. A device image and wiring diagram are shown in Fig. 1.

We perform continuous microwave reflection measurements on our device which is mounted in a dilution refrigerator with a base temperature of 30 mK. The reflected signal is homodyne demodulated with an in-phase and quadrature (IQ) mixer and the two quadratures of signal are recorded as a gapless voltage record in 3 s segments by an Alazar 9371 digitizer operating at a 300 MHz sample rate. This is downsampled to 1 MHz sample rate to ensure a sufficient signal-to-noise ratio (SNR) for our later analysis; low-power data sometimes require further downsampling to maintain an SNR greater than 3. Data were collected and processed in this way over a range of parameters: the dilution refrigerator temperature, the ABS energy, and the applied microwave power. For brevity, we restrict ourselves in this analysis to a constant power of −133 dBm (∼25 photons) at the device. This power was chosen as it gives reasonable SNR at all flux values, but is always at least 6 dB below the power at which we start to observe a power-dependent resonant frequency shift due to the nonlinearity of the nanoSQUID inductance [32]. More details on data collection are given in the Supplemental Material [35].

We take the downsampled IQ voltage record and fit it to a hidden Markov model (HMM) [36]. The HMM fits the data to two modes with Gaussian-distributed voltage emissions, corresponding to the "hidden" state of the resonance with zero or one trapped QPs. While there is evidence of periods when there are two trapped QPs, these are rare enough that they do not affect the analysis, and so we neglect them [27]. The HMM also fits a matrix of transition rates between hidden states, assuming a Markovian process of switching between states. These transition rates are parameters of the model and are used in the majority of our analysis. The fit modes and transition matrix are then used in a maximum *a posteriori* probability estimation procedure to assign a hidden state to every data point. Our HMM uses the Viterbi algorithm to perform this estimation, finding the series of hidden states that is most likely to generate the observed data. Thus we use the HMM to transform the IQ voltage time series into a

time series of the number of trapped QPs (either 0 or 1 in this analysis) and we obtain the rates of QPs trapping and clearing from the HMM fit. A more detailed explanation is given in the Supplemental Material [35].

The present Letter explores the behavior of three quantities derived from the HMM analysis as a function of ABS energy and temperature. Γ_{trap} is the rate of QPs relaxing from the bulk into available ABS of the junction, Γ_{release} is the rate of clearing QPs from ABS to the bulk, and $\bar{n}$ which we call the mean occupation is the time average of the number of trapped QPs. Γ_{trap} and Γ_{release} are found from the off-diagonal elements of the HMM transition matrix—that is, they are parameters of the model used to extract the ABS occupation time series—while $\bar{n}$ is found from averaging the extracted QP occupation time series over the full 3 s record.

We begin our modeling with the trap rate. Assuming trapping events are independent of each other and spontaneous emission dominates the QP relaxation into the ABS, each QP in the bulk has a temperature-independent trapping rate. This implies the overall trap rate is separable, $\Gamma_{\text{trap}}(\Delta_A, T) = f(\Delta_A)x(T)$, where $x(T)$ is the fractional quasiparticle density and $\Delta_A \equiv \Delta - E_A$ is the trap depth. We take the limit $\tau \to 1$ as the Dorkhov distribution $\rho(\tau)$ is sharply peaked at 0 and 1, and channels with 0 transmittivity do not contribute to the transport. The fractional quasiparticle density should be the sum of a nonequilibrium background x_{ne} and a thermal population:

$$x(T) = x_{\text{ne}} + \sqrt{\frac{2\pi k_B T}{\Delta}} \exp\left(\frac{-\Delta}{k_B T}\right). \tag{2}$$

We expect that most bulk QPs are near the gap energy, so for spontaneous emission we take $f(\Delta_A) \propto \Delta_A^3$. Putting this together, we obtain a model for the trap rate

$$\Gamma_{\text{trap}} = \beta \Delta_A^3 \left[x_{\text{ne}} + \sqrt{\frac{2\pi k_B T}{\Delta}} \exp\left(\frac{-\Delta}{k_B T}\right)\right], \tag{3}$$

where β, Δ, and x_{ne} are the free parameters. To improve the quality of our fit, we take advantage of the low-temperature saturation of the trap rate $\Gamma^0_{\text{trap}}(\Delta_A) \approx \beta \Delta_A^3 x_{\text{ne}}$ for $T \leqslant 120$ mK. We first subtract $\Gamma^0_{\text{trap}}(\Delta_A)$ from Eq. (3) and fit the resulting quantity to find the gap Δ and scaling factor β. Next we divide Eq. (3) by $\Gamma^0_{\text{trap}}(\Delta_A)$ and fit this normalized rate with the fractional nonequilibrium density x_{ne} as the only free parameter. This fitting procedure is covered in detail in the Supplemental Material [35]. In Fig. 2, we show the full model [Eq. (3)] using the combined results of this fitting procedure. We find $\beta = 8.73 \pm 0.68 \times 10^{15}$ MHz/eV^3, $x_{\text{ne}} = 8.50 \pm 0.10 \times 10^{-7}$, and $\Delta = 185.0 \pm 1.5$ μeV. We note that the fractional nonequilibrium density x_{ne} is quite high compared to recent works [2,7,8] which show a fractional density on the order of 10^{-9}. Our setup uses light-tight radiation shields on all stages of the fridge, with a Berkeley black infrared-absorbing coating [37] on the interior of the 100 mK and mixing chamber shields. In addition, the sample package is mounted inside of an Amumetal 4K shield with a tin-plated copper can nested inside, also with a Berkeley Black interior coating. We use custom-made Eccosorb filters as well as K&L 12-GHz low-pass filters on all inputs and outputs. A full diagram is available in shown in Fig. 1. We suspect that our

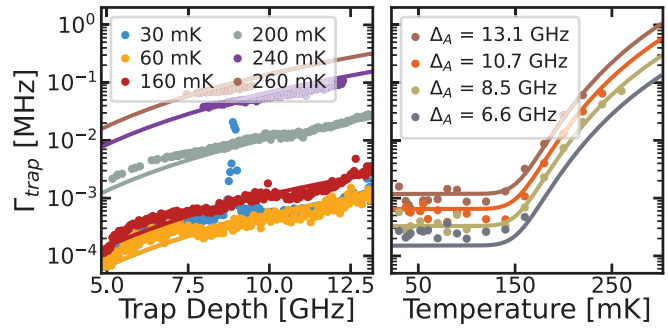

FIG. 2. Measured trap rate (circles) and model (solid lines). The dependence on the trap depth Δ_A is shown on the left, while temperature dependence is shown on the right. We note the peak in 30 mK data around 9 GHz on the left was observed as a period of significantly larger than normal mean occupation which lasted approximately 1 h in laboratory time. The source of this peak has not been found and it is not reproducible.

device geometry may contribute to the higher-than-expected density, as large areas of low-gap superconducting aluminum are galvanically coupled to the SQUID. It also may be the case that our filtering is insufficient, as recent results have shown evidence that even very extensive filtering does not fully remove stray infrared light [38]. We see no significant dependence of the trapping rate on the drive power, and so it is unlikely that our drive is generating additional QPs.

The left panel of Fig. 2 shows a peak in the 30 mK data near 9 GHz. This anomaly was present in the trap rate and mean occupation, while the release rate was marginally increased. We attribute this to a temporary increase in the bulk QP density, as repeated measurements under nearly identical conditions did not show this effect. The period of increased trapping lasted for approximately 1 h with no change in fridge conditions and no obvious environment factors to blame. We note the duration of the effect is too long to be caused by adhesive strain [39] or a strong cosmic ray [40].

We now turn our attention to Γ_{release}. To promote a trapped QP from ABS to the continuum of states above the gap, sufficient energy (at least Δ_A) must be absorbed. In a well shielded dilution refrigerator, we expect this energy to come from the absorption of phonons. The clearing rate due to electron-phonon interactions should be linear in the phonon density,

$$\Gamma_{\text{phonon}}(\Delta_A, T) \propto \rho_{\epsilon \geqslant \Delta_A}(T), \tag{4}$$

where $\rho_{\epsilon \geqslant \Delta_A}(T)$ is the density of phonons with energy exceeding the trap depth. In the Supplemental Material [35], we integrate the Debye density of states and Bose-Einstein distribution over energies exceeding the trap depth to obtain the model for QP clearing due to phonons:

$$\Gamma_{\text{phonon}}(\Delta_A, T) = \alpha T^3 \left[-\left(\frac{\Delta_A}{k_B T}\right)^2 \ln\left(1 - e^{\frac{-\Delta_A}{k_B T}}\right) + \frac{2\Delta_A}{k_B T} \text{Li}_2\left(e^{\frac{-\Delta_A}{k_B T}}\right) + 2\,\text{Li}_3\left(e^{\frac{-\Delta_A}{k_B T}}\right)\right]. \tag{5}$$

In the above, $\text{Li}_n(x)$ is the polylogarithm function of order n and $\alpha = C_{\text{ABS}\to\text{bulk}} k_B^3 / 2\pi^2 \hbar^3 v^3$ is an overall scaling factor; v

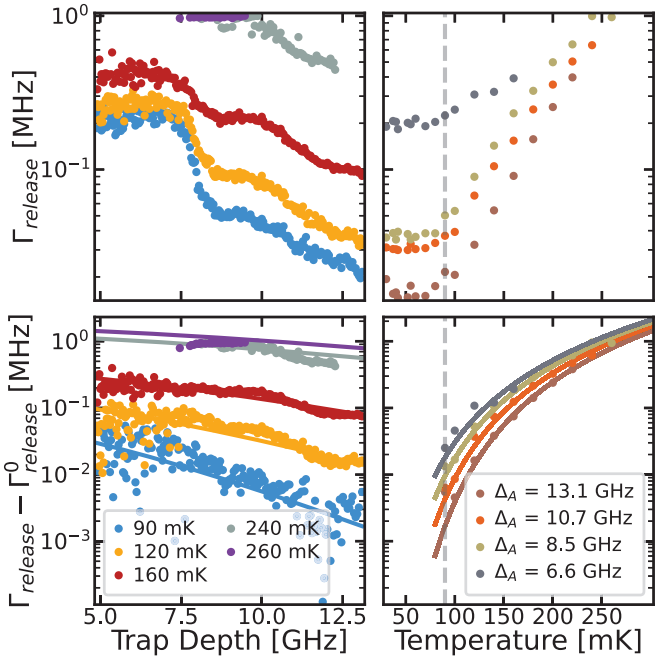

FIG. 3. Top: The measured release rate vs trap depth and temperature. The top left panel shows the structure in the trap depth dependence which is attributed to the driven electron-photon interactions which dominate at low temperature. In the top right panel, the low-temperature saturation is visible. The gray dashed line indicates the cutoff temperature (90 mK) for the fit. Bottom: The measured release rate minus the low-temperature saturation is shown as circles, while the phonon clearing model [Eq. (7)] is shown as solid curves.

is the speed of sound in our sample and $C_{\mathrm{ABS}\to\mathrm{bulk}}$ relates the ABS clearing rate to the phonon density. The formal foundation for $C_{\mathrm{ABS}\to\mathrm{bulk}}$ is a matter worthy of study as it represents the coupling between ABS and an incoherent bath.

In our measurements, we observe that the release rate saturates at $T \leqslant 60$ mK to a value which depends on the power of our microwave readout tone, suggesting that low-temperature clearing is dominated by driven electron-photon interactions. This is surprising because a single readout photon (≈4.27 GHz) has insufficient energy to clear the ABS trap [$\Delta_A(\phi) > 5$ GHz $\forall$ measured ϕ]. It may be the case that nonlinear processes in the resonator or transitions to intermediate ABS mediate this process, which will be the subject of future work. Accounting for this readout-dominated electron-photon clearing, we can model the total release rate as

$$\Gamma_{\mathrm{release}}(\Delta_A, T) = \Gamma_{\mathrm{RO}}(\Delta_A) + \Gamma_{\mathrm{phonon}}(\Delta_A, T), \tag{6}$$

where the electron-photon clearing rate Γ_{RO} is the subject of future work. For now, we take advantage of the low-temperature saturation $\Gamma^0_{\mathrm{release}} \approx \Gamma_{\mathrm{RO}}$ to eliminate this photon contribution and maintain focus on the electron-phonon clearing rate. Our model is

$$\Gamma_{\mathrm{release}}(\Delta_A, T) - \Gamma^0_{\mathrm{release}}(\Delta_A) \approx \Gamma_{\mathrm{phonon}}(\Delta_A, T), \tag{7}$$

which is equivalent to the right-hand side of Eq. (5). We keep $\Delta = 185$ μeV and fit Eq. (7) with α as the only free parameter as shown in Fig. 3. We obtain $\alpha = 38.51 \pm 0.36$ MHz/K^3. Clearly the high-temperature release rate is dominated by a thermal distribution of phonons, but this result shows that nonthermal sources may dominate at typical qubit operating temperatures. We point out that the 240 and 260 mK data in the top left panel show some clipping of the release rate data to the 1 MHz sample rate—a limitation of our measurement rather than a physical effect.

Our last feature of interest is the mean occupation $\bar{n}$, which is taken directly from the extracted time series of ABS occupations, not from HMM parameters. We start with a simple sum over weighted probabilities,

$$\bar{n} = \sum_i iP(i), \tag{8}$$

where $P(i)$ is the probability of having i trapped QPs. In this analysis, we are only distinguishing between one trapped QP and zero trapped QPs, as the incidence of two or more trapped QPs is quite rare. We can therefore assume a stationary distribution to obtain

$$P(0)\Gamma_{\mathrm{trap}} = P(1)\Gamma_{\mathrm{release}}. \tag{9}$$

Plugging (9) into (8), we obtain the model for the mean occupation:

$$\bar{n}(\Delta_A, T) = P(0)\frac{\Gamma_{\mathrm{trap}}(\Delta_A, T)}{\Gamma_{\mathrm{release}}(\Delta_A, T)}. \tag{10}$$

Unfortunately, we are unable to eliminate the driven electron-photon contribution as we did in Eq. (7) so we simply leave $\Gamma_{\mathrm{RO}}(\Delta_A)$ as a free parameter and fit each line cut along temperature separately. We normalize by dividing out the low-temperature saturation ($T \leqslant 60$ mK) to obtain the model

$$\|\bar{n}_{\Delta_A}(T)\| = \frac{1 + \frac{1}{x_{\mathrm{ne}}}\sqrt{\frac{2\pi k_B T}{\Delta}}e^{\frac{-\Delta}{k_B T}}}{1 + \alpha_M T^3\left[-\left(\frac{\Delta_A}{k_B T}\right)^2 \ln\left(1 - e^{\frac{-\Delta_A}{k_B T}}\right) + \frac{2\Delta_A}{k_B T}\mathrm{Li}_2\left(e^{\frac{-\Delta_A}{k_B T}}\right) + 2\,\mathrm{Li}_3\left(e^{\frac{-\Delta_A}{k_B T}}\right)\right]}. \tag{11}$$

We fit this independently for each trap depth, while holding $x_{\mathrm{ne}} = 8.5 \times 10^{-7}$ and $\Delta = 185$ μeV fixed. The only fit parameter is $\alpha_M \equiv \alpha/\Gamma_{\mathrm{RO}}(\Delta_A)$. The results are shown in Fig. 4. We note the characteristic dip in mean occupation for $T \in [80, 150]$ mK arises from an increased phonon population leading to faster clearing of ABS, while the rise for $T \geqslant 150$ mK is due to a large population of thermal QPs.

We may check for self-consistency in our description by examining the relationship between $\alpha_M(\Delta_A)$ and the driven

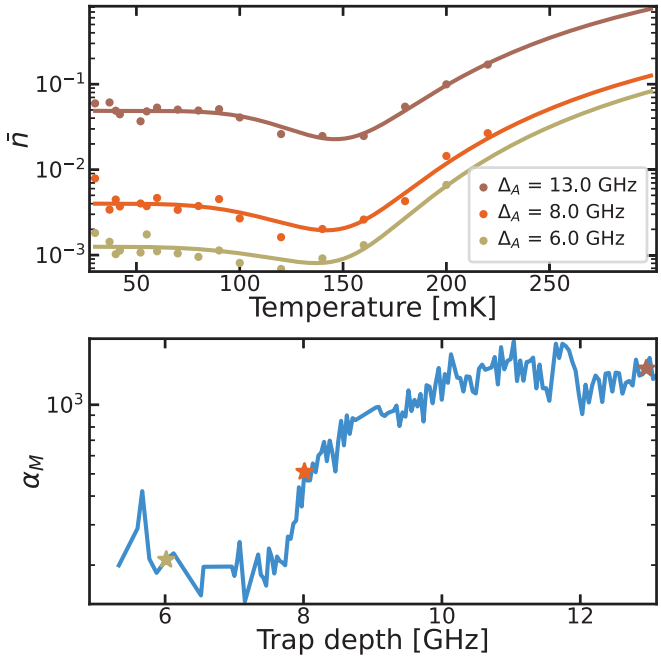

FIG. 4. Top: The measured mean occupation (circles) and the corresponding fit (solid) are shown against temperature. Note that a different fit is performed at each value of Δ_A. Bottom: The fit parameter α_M vs trap depth. Stars indicate the value of α_M for the three curves of the same color displayed in the top panel.

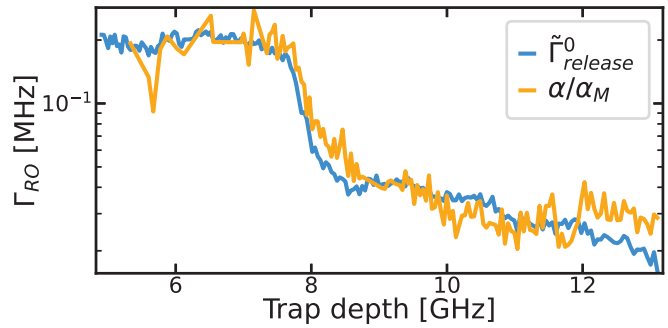

FIG. 5. Two sources of estimate for the rate of readout photons clearing QPs from the ABS traps. The measured low-temperature release rate (blue) and the fit parameter from the mean occupation, shown as α/α_M (orange), where $\alpha = 38.51$ is found from fitting the phonon contribution to the release rate as shown in Fig. 3. We point out that these agree in shape and magnitude despite coming from different sources.

electron-photon clearing rate $\Gamma_{\mathrm{RO}}(\Delta_A)$. We directly measure $\Gamma_{\mathrm{RO}}(\Delta_A)$ as the low-temperature saturation of the release rate and compare this with the estimate obtained from α/α_M, as shown in Fig. 5. Note that the former quantity comes entirely from the HMM parameters, while the latter quantity comes from a direct analysis of the ABS occupation time series. These quantities agree very closely, indicating that our analysis is robust. The driven electron-photon clearing rate has a significant structure in its dependence on Δ_A which is repeatable. There is an additional structure when one looks at the dependence on the microwave power, which is the focus of our future work with this system.

By utilizing the many ABS of aluminum nanobridge Josephson junctions, we are able to measure and explain the behavior of quasiparticle trapping in qubitlike circuits over a range of trap depth and temperature. We show that QPs relax into traps primarily by spontaneous emission of a phonon. The close agreement between our data and our model suggests that most QPs entering the trap are originally at or near the superconducting gap Δ. This indicates that any "hot" nonequilibrium quasiparticles are first relaxing to the gap in an independent process before trapping or that the majority of nonequilibrium quasiparticles exist at the gap edge, in agreement with past results [41]. We do not see any evidence of "photon-assisted trapping" (in analogy to the photon-assisted tunneling observed in tunnel junctions) where an infrared photon breaks a Cooper pair, promoting a QP directly into an ABS. This process may occur at lower rates, and is the subject of future work. We also show that clearing of QPs from ABS traps at temperatures above 90 mK occurs primarily through the absorption of phonons which are distributed according to the Debye model. Other sources, such as microwave photons, are the dominant source of ABS-clearing energy at qubit operating temperatures. Our results further elucidate the behavior of equilibrium and nonequilibrium quasiparticles in superconducting circuits.

We thank Leonid Glazman for useful discussions and the MIT Lincoln Laboratory for providing the TWPA used in these measurements. This work was funded by the AFOSR under FA9550-19-1-0060 and the NSF under DMR-1900135.

J.T.F., A.Z., and D.H. fabricated the device. J.T.F., A.Z., and S.S. performed measurements. J.T.F. and A.Z. performed the analysis. J.T.F. wrote the manuscript with input from all authors. E.M.L.-F. was the principal investigator (PI) supervising all aspects of the work.

[1] K. Serniak, M. Hays, G. de Lange, S. Diamond, S. Shankar, L. D. Burkhart, L. Frunzio, M. Houzet, and M. H. Devoret, Hot Nonequilibrium Quasiparticles in Transmon Qubits, Phys. Rev. Lett. **121**, 157701 (2018).

[2] A. P. Vepsäläinen, A. H. Karamlou, J. L. Orrell, A. S. Dogra, B. Loer, F. Vasconcelos, D. K. Kim, A. J. Melville, B. M. Niedzielski, J. L. Yoder, S. Gustavsson, J. A. Formaggio, B. A. VanDevender, and W. D. Oliver, Impact of ionizing radiation on superconducting qubit coherence, Nature (London) **584**, 551 (2020).

[3] C. D. Wilen, S. Abdullah, N. A. Kurinsky, C. Stanford, L. Cardani, G. D'Imperio, C. Tomei, L. Faoro, L. B. Ioffe, C. H. Liu, A. Opremcak, B. G. Christensen, J. L. DuBois, and R. McDermott, Correlated charge noise and relaxation errors in superconducting qubits, Nature (London) **594**, 369 (2021).

[4] J. M. Martinis, Saving superconducting quantum processors from decay and correlated errors generated by gamma and cosmic rays, npj Quantum Inf. **7**, 90 (2021).

[5] R. Barends, J. Wenner, M. Lenander, Y. Chen, R. C. Bialczak, J. Kelly, E. Lucero, P. O'Malley, M. Mariantoni, D. Sank, H.

Wang, T. C. White, Y. Yin, J. Zhao, A. N. Cleland, J. M. Martinis, and J. J. A. Baselmans, Minimizing quasiparticle generation from stray infrared light in superconducting quantum circuits, Appl. Phys. Lett. **99**, 113507 (2011).

[6] P. J. de Visser, J. J. A. Baselmans, P. Diener, S. J. C. Yates, A. Endo, and T. M. Klapwijk, Number Fluctuations of Sparse Quasiparticles in a Superconductor, Phys. Rev. Lett. **106**, 167004 (2011).

[7] K. Serniak, S. Diamond, M. Hays, V. Fatemi, S. Shankar, L. Frunzio, R. J. Schoelkopf, and M. H. Devoret, Direct Dispersive Monitoring of Charge Parity in Offset-Charge-Sensitive Transmons, Phys. Rev. Appl. **12**, 014052 (2019).

[8] E. T. Mannila, P. Samuelsson, S. Simbierowicz, J. T. Peltonen, V. Vesterinen, L. Grönberg, J. Hassel, V. F. Maisi, and J. P. Pekola, A superconductor free of quasiparticles for seconds, Nat. Phys. **18**, 145 (2022).

[9] A. D. Córcoles, J. M. Chow, J. M. Gambetta, C. Rigetti, J. R. Rozen, G. A. Keefe, M. Beth Rothwell, M. B. Ketchen, and M. Steffen, Protecting superconducting qubits from radiation, Appl. Phys. Lett. **99**, 181906 (2011).

[10] I. M. Pop, K. Geerlings, G. Catelani, R. J. Schoelkopf, L. I. Glazman, and M. H. Devoret, Coherent suppression of electromagnetic dissipation due to superconducting quasiparticles, Nature (London) **508**, 369 (2014).

[11] N. A. Court, A. J. Ferguson, R. Lutchyn, and R. G. Clark, Quantitative study of quasiparticle traps using the single-Cooper-pair transistor, Phys. Rev. B **77**, 100501(R) (2008).

[12] R.-P. Riwar, A. Hosseinkhani, L. D. Burkhart, Y. Y. Gao, R. J. Schoelkopf, L. I. Glazman, and G. Catelani, Normal-metal quasiparticle traps for superconducting qubits, Phys. Rev. B **94**, 104516 (2016).

[13] F. Henriques, F. Valenti, T. Charpentier, M. Lagoin, C. Gouriou, M. Martínez, L. Cardani, M. Vignati, L. Grünhaupt, D. Gusenkova, J. Ferrero, S. T. Skacel, W. Wernsdorfer, A. V. Ustinov, G. Catelani, O. Sander, and I. M. Pop, Phonon traps reduce the quasiparticle density in superconducting circuits, Appl. Phys. Lett. **115**, 212601 (2019).

[14] O. Rafferty, S. Patel, C. H. Liu, S. Abdullah, C. D. Wilen, D. C. Harrison, and R. McDermott, Spurious antenna modes of the transmon qubit, arXiv:2103.06803.

[15] C. Kurter, C. E. Murray, R. T. Gordon, B. B. Wymore, M. Sandberg, R. M. Shelby, A. Eddins, V. P. Adiga, A. D. K. Finck, E. Rivera, A. A. Stabile, B. Trimm, B. Wacaser, K. Balakrishnan, A. Pyzyna, J. Sleight, M. Steffen, and K. Rodbell, Quasiparticle tunneling as a probe of Josephson junction barrier and capacitor material in superconducting qubits, npj Quantum Inf. **8**, 31 (2022).

[16] X. Pan, Y. Zhou, H. Yuan, L. Nie, W. Wei, L. Zhang, J. Li, S. Liu, Z. H. Jiang, G. Catelani, L. Hu, F. Yan, and D. Yu, Engineering superconducting qubits to reduce quasiparticles and charge noise, Nat. Commun. **13**, 7196 (2022).

[17] A. Bargerbos, L. J. Splitthoff, M. Pita-Vidal, J. J. Wesdorp, Y. Liu, P. Krogstrup, L. P. Kouwenhoven, C. K. Andersen, and L. Grünhaupt, Mitigation of Quasiparticle Loss in Superconducting Qubits by Phonon Scattering, Phys. Rev. Appl. **19**, 024014 (2023).

[18] J. Aumentado, M. W. Keller, J. M. Martinis, and M. H. Devoret, Nonequilibrium Quasiparticles and 2*e* Periodicity in Single-Cooper-Pair Transistors, Phys. Rev. Lett. **92**, 066802 (2004).

[19] O. Naaman and J. Aumentado, Time-domain measurements of quasiparticle tunneling rates in a single-Cooper-pair transistor, Phys. Rev. B **73**, 172504 (2006).

[20] R. M. Lutchyn and L. I. Glazman, Kinetics of quasiparticle trapping in a Cooper-pair box, Phys. Rev. B **75**, 184520 (2007).

[21] M. D. Shaw, R. M. Lutchyn, P. Delsing, and P. M. Echternach, Kinetics of nonequilibrium quasiparticle tunneling in superconducting charge qubits, Phys. Rev. B **78**, 024503 (2008).

[22] L. Sun, L. DiCarlo, M. D. Reed, G. Catelani, L. S. Bishop, D. I. Schuster, B. R. Johnson, G. A. Yang, L. Frunzio, L. Glazman, M. H. Devoret, and R. J. Schoelkopf, Measurements of Quasiparticle Tunneling Dynamics in a Band-Gap-Engineered Transmon Qubit, Phys. Rev. Lett. **108**, 230509 (2012).

[23] M. Zgirski, L. Bretheau, Q. Le Masne, H. Pothier, D. Esteve, and C. Urbina, Evidence for Long-Lived Quasiparticles Trapped in Superconducting Point Contacts, Phys. Rev. Lett. **106**, 257003 (2011).

[24] E. Levenson-Falk, F. Kos, R. Vijay, L. Glazman, and I. Siddiqi, Single-Quasiparticle Trapping in Aluminum Nanobridge Josephson Junctions, Phys. Rev. Lett. **112**, 047002 (2014).

[25] D. G. Olivares, A. L. Yeyati, L. Bretheau, Ç. Ö. Girit, H. Pothier, and C. Urbina, Dynamics of quasiparticle trapping in Andreev levels, Phys. Rev. B **89**, 104504 (2014).

[26] M. Hays, G. de Lange, K. Serniak, D. J. van Woerkom, D. Bouman, P. Krogstrup, J. Nygård, A. Geresdi, and M. H. Devoret, Direct Microwave Measurement of Andreev-Bound-State Dynamics in a Semiconductor-Nanowire Josephson Junction, Phys. Rev. Lett. **121**, 047001 (2018).

[27] J. T. Farmer, A. Zarassi, D. M. Hartsell, E. Vlachos, H. Zhang, and E. M. Levenson-Falk, Continuous real-time detection of quasiparticle trapping in aluminum nanobridge Josephson junctions, Appl. Phys. Lett. **119**, 122601 (2021).

[28] C. Janvier, L. Tosi, L. Bretheau, Ç. Ö. Girit, M. Stern, P. Bertet, P. Joyez, D. Vion, D. Esteve, M. F. Goffman, H. Pothier, and C. Urbina, Coherent manipulation of Andreev states in superconducting atomic contacts, Science **349**, 1199 (2015).

[29] M. Hays, V. Fatemi, D. Bouman, J. Cerrillo, S. Diamond, K. Serniak, T. Connolly, P. Krogstrup, J. NygÄrd, A. Levy Yeyati, A. Geresdi, and M. H. Devoret, Coherent manipulation of an Andreev spin qubit, Science **373**, 430 (2021).

[30] R. Vijay, J. D. Sau, M. L. Cohen, and I. Siddiqi, Optimizing Anharmonicity in Nanoscale Weak Link Josephson Junction Oscillators, Phys. Rev. Lett. **103**, 087003 (2009).

[31] R. Vijay, E. M. Levenson-Falk, D. H. Slichter, and I. Siddiqi, Approaching ideal weak link behavior with three dimensional aluminum nanobridges, Appl. Phys. Lett. **96**, 223112 (2010).

[32] E. M. Levenson-Falk, R. Vijay, and I. Siddiqi, Nonlinear microwave response of aluminum weak-link Josephson oscillators, Appl. Phys. Lett. **98**, 123115 (2011).

[33] I. O. Kulik and A. N. Omel'Yanchuk, Contribution to the microscopic theory of the Josephson effect in superconducting bridges, JETP Lett. **21**, 216 (1975).

[34] O. N. Dorokhov, Transmission coefficient and the localization length of an electron in N bound disordered chains, JETP Lett. **36**, 318 (1982).

[35] See Supplemental Material at http://link.aps.org/supplemental/10.1103/PhysRevB.107.L140506 for the full experimental diagram, detailed derivation of models, and intermediate fitting procedures.

[36] L. Rabiner, A tutorial on hidden Markov models and selected applications in speech recognition, Proc. IEEE. **77**, 257 (1989).

[37] M. J. Persky, Review of black surfaces for space-borne infrared systems, Rev. Sci. Instrum. **70**, 2193 (1999).

[38] T. Connolly, P. D. Kurilovich, S. Diamond, H. Nho, C. G. Bøttcher, L. I. Glazman, V. Fatemi, and M. H. Devoret, Coexistence of nonequilibrium density and equilibrium energy distribution of quasiparticles in a superconducting qubit, arXiv:2302.12330.

[39] R. Anthony-Petersen, A. Biekert, R. Bunker, C. L. Chang, Y.-Y. Chang, L. Chaplinsky, E. Fascione, C. W. Fink, M. Garcia-Sciveres, R. Germond, W. Guo, S. A. Hertel, Z. Hong, N. Kurinsky, X. Li, J. Lin, M. Lisovenko, R. Mahapatra, A. Mayer, D. McKinsey *et al.*, A stress induced source of phonon bursts and quasiparticle poisoning, arXiv:2208.02790.

[40] L. Cardani, F. Valenti, N. Casali, G. Catelani, T. Charpentier, M. Clemenza, I. Colantoni, A. Cruciani, G. D'Imperio, L. Gironi, L. Grünhaupt, D. Gusenkova, F. Henriques, M. Lagoin, M. Martinez, G. Pettinari, C. Rusconi, O. Sander, C. Tomei, A. V. Ustinov *et al.*, Reducing the impact of radioactivity on quantum circuits in a deep-underground facility, Nat. Commun. **12**, 2733 (2021).

[41] S. Diamond, V. Fatemi, M. Hays, H. Nho, P. D. Kurilovich, T. Connolly, V. R. Joshi, K. Serniak, L. Frunzio, L. I. Glazman, and M. H. Devoret, Distinguishing parity-switching mechanisms in a superconducting qubit, PRX Quantum **3**, 040304 (2022).